

1 Experimental characterization of efficient second harmonic generation 2 of lamb wave modes in a nonlinear elastic isotropic plate

3 Kathryn H. Matlack,¹ Jin-Yeon Kim,² Laurence J. Jacobs,^{1,2,a)} and Jianmin Qu³

4 ¹Woodruff School of Mechanical Engineering, Georgia Institute of Technology, Atlanta,
5 Georgia 30332-0405, USA

6 ²School of Civil and Environmental Engineering, Georgia Institute of Technology, Atlanta,
7 Georgia 30332-0355, USA

8 ³Department of Civil and Environmental Engineering, Northwestern University, Evanston,
9 Illinois 60208, USA

10 (Received 1 October 2010; accepted 14 November 2010; published online xx xx xxxx)

11 This research experimentally characterizes the efficiency of Lamb wave mode pairs to generate the
12 cumulative second harmonic in an undamaged aluminum plate. Previous research developed the
13 theoretical framework for the characteristics of second harmonic generation of Lamb waves in
14 nonlinear elastic plates, and identified five mode types where the amplitude of the measured second
15 harmonic should increase linearly with ultrasonic wave propagation distance. The current research
16 considers one of these five mode types, Lamb wave mode pairs at the longitudinal velocity, and
17 experimentally confirms the theoretically predicted ratios of the rate of accumulation of the second
18 harmonic amplitude versus propagation distance for two different Lamb wave mode pairs. By
19 comparing these rates of accumulation, these experimental results are used to characterize the
20 measurement efficiency of the mode pairs under consideration. © 2011 American Institute of
21 Physics. [doi:10.1063/1.3527959]

23 I. INTRODUCTION

24 Previous research theoretically demonstrated that spe-
25 cific pairs of Lamb wave modes generate a cumulative sec-
26 ond harmonic wave when an originally monochromatic wave
27 is launched into a nonlinear elastic isotropic plate.¹⁻³ This
28 material nonlinearity is inherent in the crystalline structure of
29 aluminum.⁴ These Lamb wave mode pairs have the potential
30 to characterize material nonlinearity, since additional re-
31 search has shown that the second harmonic generation
32 (SHG) of Lamb waves is related to material nonlinearity and
33 fatigue damage.⁵⁻⁷ In terms of measuring material nonlinear-
34 ity, Lamb waves have advantages because they can: (1)
35 propagate over long distances, as opposed to pure longitudi-
36 nal or bulk waves that are more suitable for a through-the-
37 thickness measurement; and (2) interrogate the entire depth
38 of the material, unlike Rayleigh waves that only propagate
39 along the surface of the material. Thus, the ability to experi-
40 mentally characterize SHG of different Lamb wave modes
41 could provide a more efficient means of measuring material
42 nonlinearity.

43 Recent experimental work has investigated specific
44 Lamb wave mode pairs exhibiting SHG, although this work
45 was limited to one mode pair at time—a single mode pair at
46 the longitudinal phase velocity of the plate material in Pruell
47 *et al.*⁵ and Bermes *et al.*,⁷ and a mode pair at crossing points
48 (in the dispersion curve) in Deng *et al.*⁶ Previous research
49 using longitudinal waves has shown a direct relation between
50 the material's nonlinear parameter and SHG from an ultra-
51 sonic wave.^{8,9} Other theoretical models demonstrate a direct
52 correlation between material nonlinearity and accumulated

material damage prior to crack initiation.^{10,11} Research aimed
at measuring material nonlinearity with Lamb waves could
thus lead to improved techniques for quantitatively monitor-
ing accumulated material damage.

The objective of the current research is to experimentally
confirm the behavior theoretically predicted by Müller *et al.*¹
for the rate of accumulation of the second harmonic of dif-
ferent Lamb wave mode pairs in an undamaged 6061 T6
aluminum alloy plate. By comparing these rates of accumu-
lation, these experimental results are used to characterize the
measurement efficiency of the Lamb wave mode pairs under
consideration.

II. SHG

Following de Lima and Hamilton² and Müller *et al.*,¹
consider an isotropic, homogeneous, nonlinear elastic, and
infinite plate with stress-free boundary conditions at the sur-
face. A nonlinear equation of motion is developed from a
balance of linear momentum, the second-order constitutive
law, and the Lagrangian strain tensor

$$(\lambda + 2\mu) \nabla (\nabla \cdot \mathbf{u}) - \mu \nabla \times (\nabla \times \mathbf{u}) + \nabla \cdot \bar{\mathbf{S}} = \rho_0 \frac{\partial^2 \mathbf{u}}{\partial t^2}, \quad (1)$$

where \mathbf{u} is the displacement vector, t is time, $\bar{\mathbf{S}}$ is the non-
linear portion of the second Piola–Kirchhoff stress, and λ
and μ are Lamé's constants. The solution is formulated using
a perturbation approach, which assumes the total displace-
ment field can be expressed as the sum of the primary wave
(at frequency ω) and a secondary wave (the second harmonic
at frequency 2ω); this perturbation solution is possible since
the amplitude of the second harmonic is much smaller than
that of the primary wave. A full solution for the primary

^{a)}Electronic mail: laurence.jacobs@coe.gatech.edu.

82 wave is given in Graff.¹² The secondary wave solution is
 83 developed with a modal expansion technique.^{1,2}

84 Specific conditions must be satisfied for SHG. The first
 85 condition, referred to as *phase velocity matching*, requires
 86 equal phase velocities of the primary and the secondary
 87 waves. A second condition, referred to as *group velocity*
 88 *matching*, requires equal group velocities of the primary and
 89 secondary waves, and a third condition is nonzero power flux
 90 from the primary to the secondary wave. If all these condi-
 91 tions are satisfied, the trend of the second harmonic ampli-
 92 tude (amplitude of the secondary wave) can be described by
 93 the parameter r_s , defined as rate of accumulation of the sec-
 94 ond harmonic,

$$95 \quad \frac{A_2}{A_1^2} = z r_s, \quad (2)$$

96 where A_1 and A_2 are the measured amplitudes of the primary
 97 and secondary waves, respectively. The value of r_s depends
 98 on the specific Lamb wave mode pair under consideration,
 99 and includes other amplitude terms from the secondary wave
 100 besides the propagation distance, z and the primary wave
 101 amplitude, A_1 , squared. This r_s parameter accounts for the
 102 different rates of energy transfer between the primary and
 103 secondary waves, lumping together all the information about
 104 the second harmonic amplitude that should remain constant
 105 for a specific Lamb wave mode pair. So r_s is similar to the
 106 relative acoustic nonlinear parameter, β' , defined in previous
 107 work, and is used in this study to quantify the measurement
 108 effects that will cause differences between the theoretical and
 109 experimental values. Note that β' and the absolute material
 110 nonlinear parameter, β , have been experimentally correlated
 111 in previous research.^{5,7}

112 Two Lamb wave mode pairs with phase velocity equal to
 113 the longitudinal velocity (labeled L_1 and L_2 in Fig. 1) are
 114 selected for investigation due to ease of generation and
 115 detection—both of the primary waves in these mode pairs
 116 have the fastest group velocity at their respective frequen-
 117 cies, so they are well separated from other Lamb modes.
 118 Another advantage with these mode pairs is their higher rates
 119 of accumulation, e.g., 3.76 for the s1-s2 mode versus 2.49
 120 for the a2-s4 mode pair. A second type of Lamb wave mode
 121 pair, (labeled C_1 in Fig. 1) the crossing-points mode, is dif-
 122 ficult to generate and detect with the current experimental
 123 procedure since the other modes at these crossing points are
 124 generated much more efficiently. The critical parameters of
 125 the two selected Lamb wave mode pairs at the longitudinal
 126 velocity, labeled L_1 and L_2 , and one mode pair at crossing
 127 points, labeled C_1 (presented for comparison purposes), are
 128 given in Table I. A comparison of the theoretical values for
 129 the rate of accumulation of the second harmonic as computed
 130 in Müller *et al.*¹ is shown in Fig. 2.

131 III. METHOD

132 A. Experimental procedure

133 Lamb wave modes are excited using wedge generation^{5,7}
 134 in an undamaged 6061 T6 aluminum plate with thickness of
 135 1.6 mm. The wedge generation method is modified by cou-
 136 pling the wedge to the aluminum plate with salol (phenyl

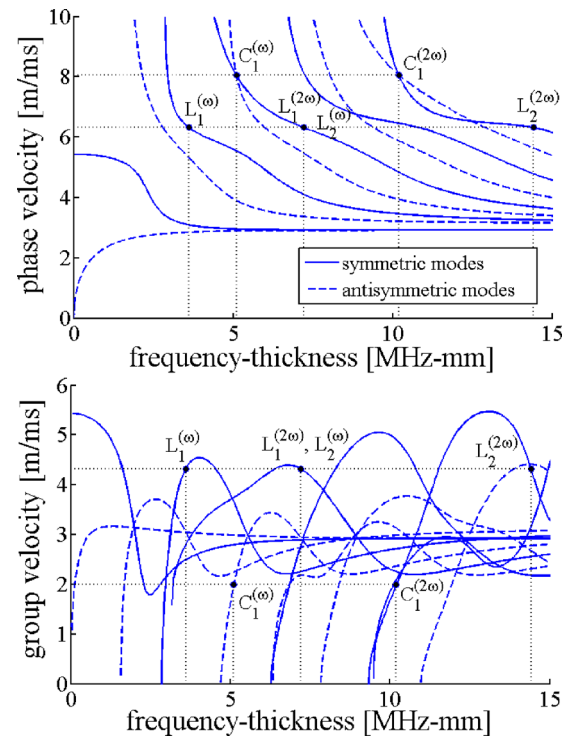


FIG. 1. (Color online) Symmetric and antisymmetric Lamb wave modes in terms of (a) phase velocity and (b) group velocity, showing experimental mode pairs (superscripts on mode pair designations distinguish between primary and secondary mode).

salicylate), producing a consistent solid-state coupling (as
 137 opposed to liquid coupling) between the wedge and plate to
 138 more efficiently generate modes with only in-plane displace-
 139 ment at the surface¹³ [i.e., $u_y(h)=0$ and $u_z(h) \neq 0$]. A liquid
 140 coupling—a thin film of oil—is chosen for the receiving
 141 wedge since the oil coupling produces less variability than
 142 the solid coupling. There is a tradeoff between variability
 143 and strength of second harmonic signal in the different types
 144 of coupling. With the fluid coupling, it is possible to detect a
 145 small amount of second harmonic displacement with much
 146 less variability. The experimental setup produces an approxi-
 147 mate phase and group velocity matching of modes (since it is
 148 difficult to physically excite a mode at a single particular
 149 frequency with the transducer setup), and this slight devia-
 150 tion excites approximate matching mode pairs that have a
 151 nonzero out-of-plane displacement at the surface. On the
 152 other hand, the solid coupling can detect the dominant in-
 153 plane displacements but with increasing variability. The re-
 154 duction in variability is chosen over strength of signal to
 155 more clearly distinguish the trend in the measured acoustic
 156 nonlinear parameter. As shown in the experimental results,
 157 the oil coupling can detect the increasing second harmonic
 158 amplitude up to a finite distance.
 159

A high-power-gated amplifier (RITEC RAM-5000 Mark
 160 IV) generates the input electrical signal of frequency either
 161 2.25 MHz or 4.5 MHz (for the s1-s2 mode pair and s2-s4
 162 mode pair, respectively) with 35 cycles for sufficient acoustic
 163 energy. The generated signal is at a voltage of 90% of the
 164 maximum power of the RITEC amplifier (~ 734 V_{pp} with
 165 transducer loading). This signal is fed into a narrowband
 166 transducer (either Panametrics X-1055 or X-1056, depending
 167

TABLE I. Summary of Lamb wave mode pair parameters. The normalized displacement of the primary mode at the surface of the plate, h , is given in terms of in-plane displacement, $\bar{u}_z(h)$, and out-of-plane (normal) displacement, $\bar{u}_y(h)$ (these displacements are normalized by the displacement of the primary wave in mode pair s1-s2; displacements are calculated with the software DISPERSE).

Mode pair	Ref.	f_d (MHz mm)	c_{ph} (m/s)	c_g (m/s)	$\bar{u}_y(h)$	$\bar{u}_z(h)$	r_s
s1-s2	L_1	3.603	6320	4326	0	1.000	3.76
s2-s4	L_2	7.206	6320	4326	0	0.499	15.05
a2-s4	C_1	5.095	8057	2000	0	0.705	2.49

168 on the mode pair) with center frequency of either 2.25 or 5
169 MHz of radius 6.25 mm and received by a narrowband trans-
170 ducer (either Panametrics A-109 or A-111) with center fre-
171 quency of either 5 or 10 MHz. The angle of the wedge is
172 designed to excite the primary wave—specifically, the angle
173 depends on the wedge material and the phase velocity of the
174 Lamb wave mode to be generated. The receiving transducer
175 simultaneously detects the primary and secondary wave am-
176 plitudes (\bar{A}_1 and \bar{A}_2 , respectively). The center frequency of
177 the receiver matches the frequency of the secondary wave
178 (2ω), thus increasing the signal-to-noise ratio (SNR) while
179 still detecting the primary wave at a frequency of ω ; the
180 amplitude of the primary wave is inherently much larger than
181 the second harmonic (amplitude of the secondary wave). The
182 measured time-domain signal is transferred to an oscillo-
183 scope, averaged 1000 times to further improve the SNR, and
184 then transferred to a PC for post digital processing. All mea-
185 surements are taken in the far-field, at propagation distances
186 of 20 to 50 cm at increments of 2.5 cm. Each measurement is
187 repeated three times, and the receiving wedge is completely
188 removed and reattached between each measurement (note
189 that the transmitting wedge remained attached to the plate
190 throughout the entire measurement set to reduce variability).

191 B. Signal processing

192 A crucial issue with nonlinear Lamb wave measurements
193 is how to accurately extract the amplitudes of the primary
194 and secondary waves from an experimentally measured time-
195 domain signal. Lamb waves are dispersive and multimodal,
196 and it is difficult to experimentally excite only one mode.
197 This research uses a time-frequency representation,^{5,7} the
198 short-time Fourier transform (STFT). For example, represen-
199 tative time slices at the first (ω) and second harmonic (2ω)

frequencies of a typical measurement that show the ampli- 200
tudes of the primary and secondary waves, \bar{A}_1 and \bar{A}_2 , is 201
provided in Fig. 3. 202

The question arises as to what signal processing param- 203
eters to use in the STFT analysis, and how to determine these 204
parameters for different Lamb wave mode pairs, not simply 205
the Lamb wave mode pairs investigated in this analysis. The 206
window size greatly affects the extracted amplitudes of the 207
measured Lamb waves—a very narrow window size has 208
greater resolution in the time domain but poor resolution in 209
the frequency domain, and the opposite is true of a very wide 210
window. Previous experimental work on the s1-s2 mode pair 211
used a narrow window size, since these modes arrived first in 212
time⁵ but this is not necessarily the case with all Lamb wave 213
mode pairs. Therefore, a more robust procedure is devel- 214
oped. 215

The measured parameter, \bar{A}_2/\bar{A}_1^2 , is inherently dominated 216
by the primary wave amplitude (since this term is squared), 217
so it is crucial that the primary wave amplitude extracted 218
from the STFTs is not adversely influenced by the signal 219
processing parameters. Since the primary wave amplitude is 220
simply a linear ultrasonic wave propagating through a wave- 221
guide, the trend of its amplitude over propagation distance 222
can be predicted with a diffraction model through a plate that 223
accounts for geometric effects of a finite source and 224
receiver—in this case the transducer/wedge assembly. If the 225
primary wave amplitude follows the expected trend, it is 226
confirmed that the primary wave amplitude is extracted cor- 227
rectly. To model this trend, the solution for a time harmonic 228
point source in an arbitrary direction is modified to model 229
the transducer/wedge assembly.¹⁴ This solution, detailed in 230
Achenbach and Xu,¹⁴ decomposes the point source into hori- 231
zontal and vertical components, and develops a modal ex- 232
pansion solution in terms of symmetric and antisymmetric 233

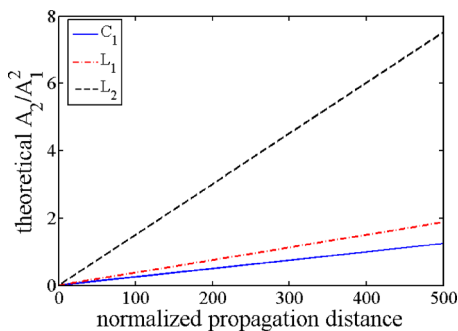


FIG. 2. (Color online) Theoretical comparison of rate of accumulation of the second harmonic of selected mode pairs.

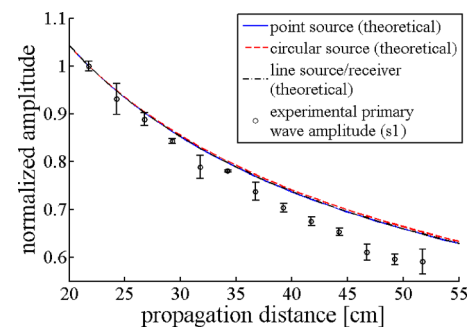


FIG. 3. (Color online) Time slices of s2-s4 received signal at a propagation distance of $z=35$ cm at the first and second harmonic frequency.

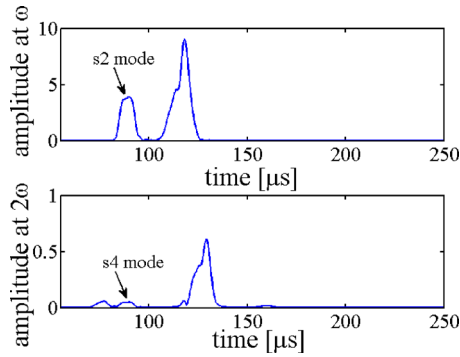


FIG. 4. (Color online) Measured primary wave amplitude of s1-s2 mode pair and the diffraction model for a point source, a circular source, and a line source/receiver.

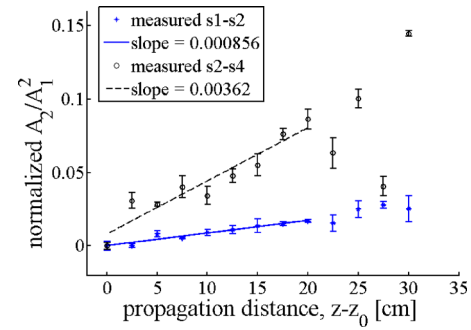


FIG. 5. (Color online) Comparison of experimental β' for s1-s2 and s2-s4 mode pairs. The ratio of the measured rate of accumulation is 4.23.

234 Lamb wave modes. While numerical integration schemes
235 make a close approximation of the experimental excitation
236 difficult, this study shows that different geometric cases, spe-
237 cifically a circular source or a line source/receiver, have
238 very little deviation from the point source solution (in terms
239 of normalized amplitude) in the far field. An example of how
240 the diffraction models, in terms of a point source, a circular
241 source, and a line source/receiver, correlate to the experi-
242 mentally measured results is given in Fig. 4.

243 Finally, differences in the primary wave amplitude of
244 different mode pairs due to frequency and signal processing
245 effects must be taken into account. The primary mode am-
246 plitude from each mode pair must be normalized to account
247 for diffraction effects at different frequencies. Since the de-
248 scribed procedure for determining the signal processing pa-
249 rameters could warrant different window sizes for different
250 Lamb wave modes pairs, the amplitudes must be normalized
251 to account for the window size in order to accurately com-
252 pare measurements of different Lamb wave mode pairs.

253 C. Measurement analysis

254 In order to relate the measured amplitude ratio, \bar{A}_2/\bar{A}_1^2 , to
255 the theoretical rate of accumulation, r_s , the influence of any
256 experimental variations must be accounted for. The ampli-
257 tude ratio has the form

$$258 \quad \frac{\bar{A}_2}{\bar{A}_1^2} = z\beta' - \beta_0, \quad (3)$$

259 where β' is the relative nonlinear parameter and β_0 is the
260 extraneous measurement nonlinearity inherent to the experi-
261 mental setup and procedure. The relative nonlinear parameter
262 is found by taking the slope of linear fit of the amplitude
263 ratio over propagation distance. To isolate the rate of accu-
264 mulation from measurement nonlinearity, the following nor-
265 malization is used on the amplitude ratio:

$$266 \quad \left(\frac{\bar{A}_2}{\bar{A}_1^2}\right)_{norm} = \left(\frac{\bar{A}_2}{\bar{A}_1^2}\right)_z - \left(\frac{\bar{A}_2}{\bar{A}_1^2}\right)_{z_0} = \beta'(z - z_0). \quad (4)$$

IV. RESULTS AND DISCUSSION 267

A. Experimental results 268

The measured (normalized) amplitude ratio, $(\bar{A}_2/\bar{A}_1^2)_{norm}$, 269
over (normalized) propagation distance for both the s1-s2 270
mode pair and s2-s4 mode pair is shown in Fig. 5. The error 271
bars show the measured standard deviation of the three mea- 272
surement sets. The linear increase over propagation distance 273
can be seen up to a propagation distance of 42 cm in both 274
measurement sets, after which there is no clear trend. 275

The s1-s2 measurements show that two unwanted modes 276
are generated—the a1 and a2 modes—though neither influ- 277
ence the primary nor secondary wave amplitudes. Out of all 278
possible modes at the first and second harmonic frequencies 279
(ω and 2ω), the primary and secondary wave modes have the 280
fastest group velocity, giving sufficient modal separation be- 281
ginning around 20 cm. The s1-s2 mode pair also has the 282
advantage of having the lowest first harmonic frequency out 283
of all the mode pairs shown in Müller *et al.*¹ to exhibit SHG. 284
This is an advantage because fewer modes occur at lower 285
frequencies. For example, five modes occur at the primary 286
frequency ($f_1=2.25$ MHz) whereas eight modes occur at the 287
secondary frequency ($f_2=4.5$ MHz). 288

The s2-s4 measurements show that three unwanted 289
modes are excited—the a2, s3, and s5 modes. The s3 mode 290
slightly influences the primary wave amplitude, since the 291
portion of the s3 mode that is close in frequency to the pri- 292
mary wave propagates with the same group velocity. How- 293
ever the primary wave is more strongly excited than the s3 294
mode, so its influence is small. Note that the secondary 295
wave, s4, does not propagate with the fastest group velocity 296
of modes at the frequency 2ω . The secondary wave ampli- 297
tude, \bar{A}_2 , as shown in Fig. 3, is located using the theoretical 298
time of arrival. 299

B. Comparison of mode pairs 300

The ratio between measured relative nonlinear param- 301
eters of the s2-s4 and s1-s2 mode pairs, 302

$$\frac{(\beta')_{s2-s4}}{(\beta')_{s1-s2}}, \quad (5) \quad 303$$

is 4.23, as shown in Fig. 5, and the theoretical ratio, 304

$$305 \quad \frac{(r_s)_{s2-s4}}{(r_s)_{s1-s2}}, \quad (6)$$

306 is 4.00, as calculated using the model in Müller *et al.*¹ It can
 307 be shown that the ratio of four comes from the dependence
 308 of the second harmonic amplitude on frequency, that is, A_2
 309 $\propto \omega^2$. The experimental ratio takes into account differences in
 310 transducer generation efficiency (note that a different set of
 311 transducers was used for the s1-s2 measurements and the
 312 s2-s4 measurements), signal processing effects, and attenua-
 313 tion in the Plexiglas wedges at different frequencies while
 314 other variations such as those associated with the coupling
 315 are difficult to quantify and thus produce some error. The
 316 experimentally measured ratio is in good agreement with the
 317 theory, further confirming the suitability of both mode pairs
 318 for SHG. While the s1-s2 Lamb wave mode pair is a better
 319 choice for SHG with the current experimental technique due
 320 to excitation of fewer modes and less influence from these
 321 modes on the primary and secondary wave amplitudes, the
 322 higher rate of accumulation with the s2-s4 mode shows that
 323 an improved experimental technique with this Lamb wave
 324 mode pair could have higher SHG efficiency. Finally, it is
 325 interesting to note that these experimental results suggest
 326 that the absolute nonlinearity parameter of Lamb waves
 327 should be in the form, $\beta \propto A_2/(z\omega^2 A_1^2)$, which is exactly the
 328 same form as in the case of longitudinal^{8,15,16} and Rayleigh
 329 waves.¹⁷⁻¹⁹ While this form has been used for Lamb waves,⁷
 330 it has not been proven theoretically, nor has it been postu-
 331 lated based on experimental evidence.

332 V. CONCLUSION

333 This research experimentally investigates two Lamb
 334 wave mode pairs that exhibit SHG, the s1-s2 mode pair and
 335 the s2-s4 mode pair. It has been theoretically shown that
 336 there is a possibility of five different types of Lamb wave
 337 mode pairs that generate the cumulative second harmonic,
 338 and as of yet a comparison of feasibility and practicality of
 339 these Lamb wave mode pairs has not been reported in the
 340 literature. For each mode pair, the primary mode is generated
 341 in an aluminum plate using the wedge/transducer method
 342 and a solid coupling to efficiently excite the pure in-plane
 343 displacements at the surface. A wedge/transducer detection
 344 method simultaneously receives the primary and secondary
 345 modes at increasing propagation distances.

Both Lamb wave mode pairs show the expected linear
 increase in the relative nonlinear parameter with propagation
 distance up to sufficiently far propagation distance (42 cm).
 Experimental results show the ratio of the relative nonlinear
 parameter of the s2-s4 mode pair to that of the s1-s2 mode
 pair is 4.23, which is in good agreement with the theoret-
 ically predicted ratio of rates of accumulation. The s1-s2
 mode pair shows fewer unwanted modes generated with no
 influence on the measured amplitudes, so this mode pair is
 preferred with the current experimental technique. However,
 since the s2-s4 mode pair shows an experimental rate of
 accumulation of the second harmonic (β') four times higher
 than the s1-s2 mode pair, the s2-s4 mode pair could be used
 with a higher efficiency with an improved experimental
 method.

ACKNOWLEDGMENTS

This work was partially supported by the National Sci-
 ence Foundation through a Graduate Research Fellowship to
 Kathryn Matlack and by the Air Force Office of Scientific
 Research under Contract No. FA9550-08-1-0241.

- ¹M. F. Müller, J.-Y. Kim, J. Qu, and L. J. Jacobs, *J. Acoust. Soc. Am.* **127**, 2141 (2010). 366
- ²W. J. N. de Lima and M. F. Hamilton, *J. Sound Vib.* **265**, 819 (2003). 367
- ³A. Srivastava and F. Lanza di Scalea, *J. Sound Vib.* **323**, 932 (2009). 368
- ⁴J. H. Cantrell, *J. Appl. Phys.* **76**, 3372 (1994). 369
- ⁵C. Pruell, J.-Y. Kim, J. Qu, and L. J. Jacobs, *NDT Int.* **42**, 199 (2009). 370
- ⁶M. Deng, P. Wang, and X. Lv, *J. Phys. D: Appl. Phys.* **38**, 344 (2005). 371
- ⁷C. Bermes, J.-Y. Kim, J. Qu, and L. J. Jacobs, *Mech. Syst. Signal Process.* **22**, 638 (2008). 372
- ⁸J. H. Cantrell and W. T. Yost, *Int. J. Fatigue* **23**, Suppl. 1, 487 (2001). 373
- ⁹W. T. Yost and J. H. Cantrell, *Proc.-IEEE Ultrason. Symp.* **2**, 947 (1992). 374
- ¹⁰J. H. Cantrell, *Proc. R. Soc. London, Ser. A* **460**, 757 (2004). 375
- ¹¹J.-Y. Kim, J. Qu, L. J. Jacobs, J. W. Littles, and M. F. Savage, *J. Nonde-struct. Eval.* **25**, 29 (2006). 376
- ¹²K. F. Graff, *Wave Motion in Elastic Solids* (Oxford University Press, London, 1975). 377
- ¹³E. P. Papadakis, *J. Appl. Phys.* **35**, 1474 (1964). 378
- ¹⁴J. D. Achenbach and Y. Xu, *J. Acoust. Soc. Am.* **106**, 83 (1999). 379
- ¹⁵J.-Y. Kim, L. J. Jacobs, J. Qu, and J. W. Littles, *J. Acoust. Soc. Am.* **120**, 1266 (2006). 380
- ¹⁶A. N. Norris, in *Nonlinear Acoustics*, edited by M. F. Hamilton and D. T. Blackstock (Academic, New York, 1998). 381
- ¹⁷M. Liu, J.-Y. Kim, L. J. Jacobs, and J. Qu, *NDT Int.* **■**, **■** (2010). 382
- ¹⁸J. Herrmann, J.-Y. Kim, L. J. Jacobs, J. Qu, J. W. Littles, and M. F. Savage, *J. Appl. Phys.* **99**, 124913 (2006). 383
- ¹⁹J. L. Blackshire, S. Sathish, J. Na, and J. Frouin, in *Review of Progress in Quantitative Nondestructive Evaluation*, edited by D. O. Thompson and D. E. Chimenti (AIP, USA, 2003), p. 1479. 384

365 AQ:
#3389 AQ:
#4

AUTHOR QUERIES — 022101JAP

- #1 Au: Please verify the changes made from “Mueller” to “Müller” in text throughout.
- #2 Au: Please define “PC” if possible.
- #3 Au: Please supply Grant No. for “National Science Foundation” if possible.
- #4 Au: Please supply volume number and page number in Ref. 17.